Journal of Thermal Analysis and Calorimetry (2023) 148:1149–1162
https://doi.org/10.1007/s10973-022-11721-w

Energy and exergy analysis of a modified three-stage auto-cascade refrigeration cycle using low-GWP refrigerants for sustainable development

Yanbin Qin[1] · Nanxi Li[2] · Hua Zhang[1] · Baolin Liu[1]

Received: 29 July 2022 / Accepted: 15 October 2022 / Published online: 7 December 2022

Abstract

This study proposed a modified three-stage auto-cascade refrigeration cycle (MTARC) operating with environmentally benign zeotropic mixture of R1234yf/R170/R14 at the refrigeration temperature level of − 80 °C. Compared with the conventional three-stage auto-cascade refrigeration cycle (CTARC), MTARC incorporates an additional pressure regulator between the condenser and separator to realize phase separation at a lower pressure and temperature. A comprehensive evaluation of energy and exergy performance of the two cycles was conducted theoretically. Under a typical working condition, the cooling capacity, COP and exergy efficiency of the MTARC are improved by 15.85%, 11.69% and 7.65% in comparison with the CTARC, respectively. In addition, a lower evaporating temperature was also obtained by the MTARC under the same operating condition. When the intermediate pressure drops from 2 to 1 MPa, the cooling capacity, COP and exergy efficiency are improved by 35.43%, 25.25% and 16.74%, respectively, for the MTARC, meanwhile the compressor outlet temperature increases 19.93 °C from 92.27 to 112.20 °C. Therefore, the selection of the intermediate pressure should be comprehensively considered to ensure a desirable cycle performance and a proper working condition for the compressor. The proposed modified cycle offers new pathways for designing innovative cryogenic refrigeration systems, thereby potentially improving the energy economy in a myriad of modern energy applications for sustainability concerns.

Keywords Energy · Exergy · Three-stage ARC · Thermodynamic · Intermediate pressure

Abbreviations

CTARC	Conventional three-stage auto-cascade refrigeration cycle
CE	Condensing evaporator
COP	Coefficient of performance
EV	Expansion valve
GWP	Global warming potential
h	Specific enthalpy (kJ/kg)
MTARC	Modified three-stage auto-cascade refrigeration cycle
$\dot{m}$	Mass flow rate (kg s^{-1})
NBP	Normal boiling point
ODP	Ozone depletion potential
p	Pressure (MPa)
$\dot{Q}$	Cooling capacity (kW)
q	Vapor quality
s	Specific entropy (kJ/kg K^{-1})
T	Temperature (°C)
$\dot{W}$	Input power (kW)
Z	Initial composition

Greek letters

β_D	Exergy destruction percentage (%)
η	Isentropic efficiency
$\dot{\chi}_D$	Exergy destruction (kW)
ψ	Exergy efficiency
Δ	Difference

Subscripts

0	Reference state
1, 2, …, 17	State points
com.	Compressor
con.	Air-cooled condenser
eva.	Evaporator

✉ Yanbin Qin
qyb110714@usst.edu.cn

[1] University of Shanghai for Science and Technology, Shanghai 200093, People's Republic of China

[2] Chinese Academy of Science, Shanghai Institute of Technical Physics, Shanghai 200083, People's Republic of China

Introduction

With the development of industry and society, the attainment of low temperatures below − 50 °C has drawn more and more attentions in many fields [1]. In recent years, in response to the current COVID-19 pandemic, the ultra-low temperature (UTL) around − 80 °C is increasingly demanded in biomedical areas such as the cryopreservation of new vaccines and cryosurgery. Economical refrigeration in the ULT range cannot be achieved with standard single-stage systems because of the required high compression ratio, which leads to a low efficiency and high discharge temperature [2]. Principally, temperatures below − 40 °C can be obtained by multi-stage compression refrigeration cycles, cascade refrigeration cycles and auto-cascade refrigeration cycles (ARC) [3]. Among these applications, the ARC systems have been extensively used because of their simple structure, high reliability, low cost and high thermodynamic efficiency [4]. In recent decades, energy shortage and environmental pollution have become progressively severe, calling for more utilizations of the ARC system which is higher in refrigeration efficiency and more environmentally friendly [5]. Thus, much effort has been made on improving the ARC systems, which mainly includes two aspects: to improve the structure of the existing ARC systems, and to look for mixed refrigerants that can meet the needs of environmental protection and exhibit high thermodynamic efficiency as well [6].

In terms of structural optimization of refrigeration systems, the ejector was found to be able to convert the pressure energy of the refrigerant into kinetic energy and then return to pressure energy, thereby recovering the throttling loss and improving the system efficiency [7–11]. Hao et al. [12] proposed a novel hybrid auto-cascade refrigeration system coupled with an ejector cycle. This hybrid cycle effectively saves high-grade electric energy or mechanical energy by the ejector driven by low-grade thermal energy such as waste heat and solar energy. It was found that the ejector can reduce the compressor input power by 50%. Yu et al. [13] studied the performance of an ejector-enhanced two-stage ARC and found that the modified system can effectively improve the coefficient of performance (COP). When using R23/R134a as the working fluid, the pressure ratio of compressor was reduced by 25.8% and the COP was improved by 19.1% over the conventional ARC. Similarly, Bai et al. [14, 15] also studied a two-stage ARC, and results show that by adding an ejector to the system can boost the exergy efficiency and COP by 25.1% and 9.6%, respectively. Rodríguez-Jara et al. [2] used an ejector as the expansion valve in ARC and found that the COP was increased by 12%. This study also indicates that the mixture of R1150/R600a is a suitable combination for ARC.

As for other aspects of system structure optimization, a double internal ARC system was introduced by Cheng et al. [16], and the authors concluded that the modified system can effectively increase the mass flow of the low boiling point component entering the evaporator, and further improve the system performance. Compared with the flash tank system, the proposed system shows a 9.6% higher heating capacity and a 6.1% higher COP. Chen et al. [17] used two separators in a modified ARC to achieve partial-condensation separation, and used the corresponding capillary tubes to get flash separation for a composition shift effect. Under the given operation conditions, the cycle performance improvement of the modified system in terms of COP, volumetric cooling capacity and exergy efficiency can reach up to 12.7%, 32.6% and 20%, respectively. Similar optimizations also concluded that the modified cycle can improve the cycle performance due to the composition shift effect of the zeotropic mixture during the flash separation process [18, 19]. The results show that the maximum COP of the modified system with R290/R600a and R134a/R236fa can be improved by 26.7% and 18.6%, respectively [19]. A modified ARC with a fractionation heat exchanger was experimentally studied by Zhang et al. [20]. It was found that the corresponding refrigeration capacity, power input and COP were reduced by 37.1–61.7%, 24.7–36.8% and 16.4–42.7%, respectively. Chen et al. [21] concluded that the addition of the subcooler in the ARC could improve both the energy and exergy performances, and the COP, volumetric cooling capacity and exergy efficiency of the modified cycle can be improved by up to an average of 37.5%, 42.3% and 34.3% compared to those of the basic cycle, respectively. Liu et al. [22] introduced an auxiliary separator into a conventional ARC, and found that the overall performance of the modified system was higher. Under a typical operating condition, the improvements of COP and exergy efficiency were increased by 16.1% and 10.23% respectively, and the overall cost rate was decreased by 2.51%. Research on the structural optimization and efficiency improvement of the energy systems was also carried out by Toghraie and co-workers [23–29]. Asgari et al. [30] used R600 as the refrigerant in an internal ARC, and all heat exchangers were modeled by taking pressure drops into consideration. The multi-objective optimization indicated that the improvements of total avoidable exergy destruction rate, total avoidable investment and total avoidable exergy destruction cost rates were 76.78%, 38.66% and 103.38%, respectively. Yan et al. [31] used R290/R600a as refrigerants in an internal ARC. The simulation results show that the internal ARC has 7.8–13.3% improvement in COP, 10.2–17.1% improvement in volumetric refrigeration capacity and 7.4–12.3% reduction in pressure ratio of compressor.

On the other hand, the environmentally benign refrigerants with low GWP values are used for the sustainability of

ARC equipment [32]. Mota-Babiloni et al. [1] summarized the recent developments in ultra-low temperature refrigeration systems and working fluids, and concluded that the HC refrigerants of R170 and R1150 are the best solutions. Aprea and Maiorino [33] achieved − 150 °C in a space of 0.25 m^3 for a medical application by using a mixture of R507, R245fa, R116, R23, R14, R740 and R290. Wang et al. [4] theoretically investigated the system performance of a two-stage ARC using six binary mixtures and concluded that the R170/R600 (0.55/0.45) was an ideal substitute at − 60 °C. Sivakumar and Somasundaram [34, 35] experimentally investigated a three-stage ARC using R290/R170/R14, R290/R23/R14 and R1270/R170/R14 and found that the system operating with R290/R23/R14 showed a better performance. Qin et al. [36] theoretically analyzed the thermodynamic characteristics of a three-stage ARC using four ternary mixtures composed of R1234yf, R1132a, R23, R41, R170 and R14. The results show that all the three medium-temperature alternatives of R1132a, R41 and R170 could be good drop-in replacements for R23. The COP and exergy efficiency of the ARC operating with R1234yf/R41/R14 with the mass fraction of 0.64/0.17/0.19 were 0.2713 and 13.91% at − 100 °C, respectively. Kilicarslan and Hosoz [37] studied the thermodynamic performance of a two-stage ARC using R404a/R23, R234a/R23, R152a/R23, R717/R23, R507/R23 and R290/R23. It was found that the R717/R23 system and R507/R23 system showed the highest and the lowest COP, respectively. Lizarte et al. [38] used R152a to replace R134a in the ARC system. The highest COP and exergy efficiency were 0.79 and 31.6% corresponding to organic Rankine cycle evaporation temperatures of 315 °C and 255 °C, respectively. Liu et al. [39] proposed a modified two-stage ARC with a self-recuperator. The energy and exergy analysis indicated that the COP of the modified ARC was increased by 6.24% and 24.17% when using R290/R170 and R600a/R1150, respectively. It was also found for the modified ARC that COP and refrigeration capacity were positively correlated with intermediate pressure. A zeotropic mixture of R600a/R744 was employed as a working fluid in an ARC system by Sobieraj [40]. It was found that the working mass concentration of R744 was higher, since it was closer to the nominal concentration and the discharge pressure was lower by 19% to even 39% when a recuperative heat exchanger was employed in the system. An increase of up to 20% in the COP was observed. Rui et al. [41] proposed a novel ternary mixture, R600a/R23/R14, for ARC systems for 190 K applications. The results demonstrated the feasibility of the proposed R600a/R23/R14 ternary mixture as an environmental benign alternative for ARC systems, and a mass ratio of 35/30/35 mixture was recommended. He et al. [42] studied the theoretical performance of a two-stage ARC system using R170/R600a, R170/R600, R1150/R600a, R1150/R600, and R23/R134a. The results showed that R170/R600 showed the best performance, and the exergy loss ratios of the heat exchanger in the R170/R600 and R23/R134a systems were the highest at 52.3% and 56.7%, respectively. A comparison study was conducted by Hamad et al. [43] to investigate the performance of an ARC using R290 and R600a. R290/R600a with four mass ratios (70/30, 60/40, 50/50 and 40/60) was used to investigate the performance of the system and compared with R134a. Results show that the mixed refrigerant with the mass fraction of 60/40 displayed a higher performance comparing with other mass fractions and R134a. Also, a 29% increase in COP and a 26% increase in refrigeration effect were achieved, respectively.

Generally, the low separation efficiency is an important reason for the poor performance of the ARC systems. It is seen from the literature review outlined above that the studies related to the energy and exergy analysis of the ARC have been based on the perspective of cycle structure modification to improve separation efficiency, in which the decrease of refrigerant flow to evaporator was not taken into account [18, 20]. On the other hand, some studies mentioned these effects without performing a detailed cycle analysis, especially for the three-stage ARC. To solve this problem, this paper proposed a modified three-stage ARC (MTARC) with an additional expansion valve installed between the condenser and the vapor–liquid separator for refrigeration applications at ultra-low temperatures around − 80 °C. The pressure regulator can effectively increase the refrigerant flow to the evaporator but has little effect on its composition (maintain a high separation efficiency), thereby the system performances can be further improved. Under consideration of the environmental issues and the process of sustainable development, the experimentally benign ternary mixture of R1234yf/R170/R14 with low GWP value was selected as the working fluid. This study is different from the ones in the literature because it presents a detailed first and second law analysis of the MTARC in comparison with the conventional three-stage ARC (CTARC) under various operating characteristics. The proposed MTARC offers new pathways for designing energy-efficient cryogenic refrigeration systems and applications that operate below − 80 °C for sustainable development.

Mathematical model of the modified three-stage ARC

Cycle description

Figure 1a and b are the schematic diagram and the lg*p*-*h* diagram for the MTARC operating with R1234yf/R170/R14, respectively. Compared with the MTARC, the structure of the CTARC doesn't have the expansion valve between the condenser and the vapor–liquid separator, so the schematic

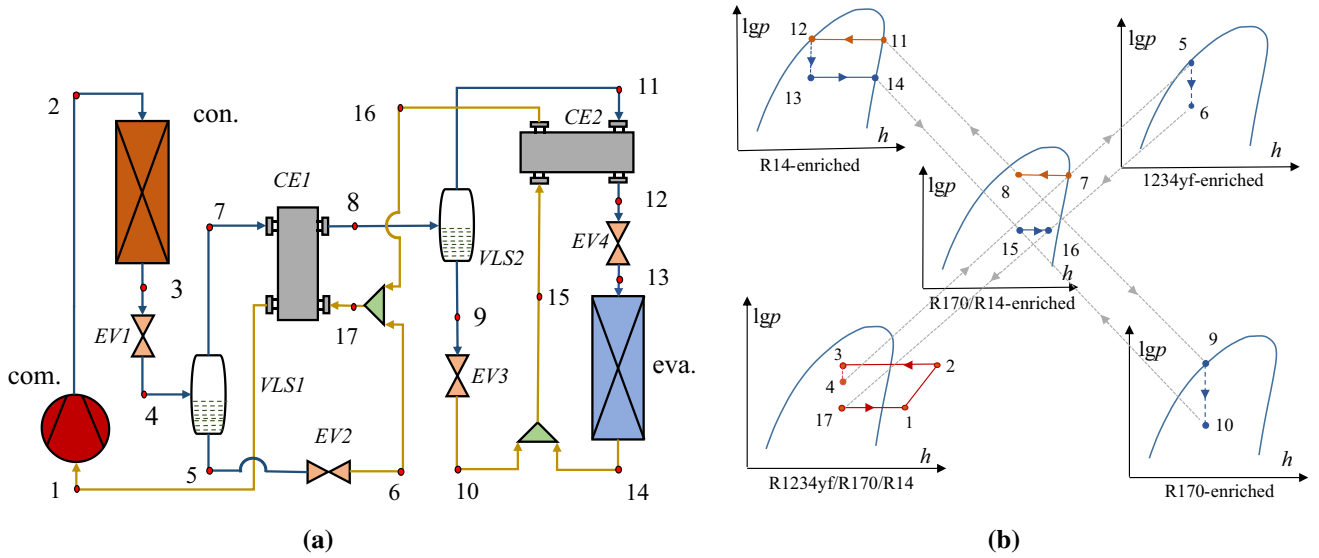

Fig. 1 **a** The schematic diagram of the MTARC; **b** The schematic lg*p*-*h* diagram of the MTARC

diagram of the CTARC is not given again. For the MTARC, the zeotropic mixture from the compressor is partially condensed in the condenser. After that, the two-phase refrigerant is expanded in the first expansion valve *EV1*, and then enters the first vapor–liquid separator *VLS1*. The R1234yf-enriched liquid flows out from the bottom of *VLS1*, and the R170/R14-enriched vapor flows out from the top of *VLS1*. The saturated vapor at state point 7 is partially condensed in the first condensing evaporator *CE1* and then enters the second vapor–liquid separator *VLS2*. At state point 5, the saturated liquid expands to vapor–liquid fluid by the second expansion valve *EV2*.

The R14-enriched vapor coming out from the top of *VLS2* is condensed efficiently in the second condensing evaporator *CE2*. After the pressure decreases in the fourth expansion valve *EV4,* the R14-enriched refrigerant becomes vapor–liquid state and then fully evaporates in the evaporator. The R170-enriched liquid out from the bottom of *VLS2* is expanded to vapor–liquid fluid by the third expansion valve *EV3*. Afterwards, it mixes with the refrigerant exiting from the evaporator, and then the mixture cools the saturated vapor in *CE2*. After leaving *CE2*, the mixture at state point 16 mixes with the two-phase refrigerant out from *EV2*. The mixture at state point 17 cools the saturated vapor in *CE1* and then is sucked into the compressor.

Thermodynamic model

To facilitate the calculations, some assumptions are adopted as follows [44]:

(a) The system operates in steady state;
(b) The throttling processes are considered to be isenthalpic;
(c) The compression process is isentropic and irreversible;
(d) The heat losses in pipelines and equipment are neglected, and the pressure drop in the pipelines and heat exchangers is negligible.
(e) Fluid exiting the phase separator is considered to be saturated. The mixture at state point 12 is saturated liquid.
(f) The kinetic exergy and potential exergy of the refrigerant are ignored.

Energy and exergy balance

The governing equations of the system components satisfy the mass and energy conservation equations. The general expressions are as follows:

Mass conservation:

$$\sum \dot{m}_{\text{in}} = \sum \dot{m}_{\text{out}} \tag{1}$$

Energy conservation:

$$\sum \dot{Q} = \sum \dot{m}_{\text{out}} h_{\text{out}} - \sum \dot{m}_{\text{in}} h_{\text{in}} + \sum \dot{W} \tag{2}$$

The COP of the ARC can be determined by:

$$\text{COP} = \frac{\dot{Q}_{\text{eva.}}}{\dot{W}_{\text{com.}}} \tag{3}$$

Incorporating the second law of thermodynamics, the general expression of the exergy conservation equation of each system component can be expressed as:

$$\dot{\chi}_{\mathrm{D}} = \sum \dot{m}_{\mathrm{in}}\dot{\chi}_{\mathrm{in}} - \sum \dot{m}_{\mathrm{out}}\dot{\chi}_{\mathrm{out}} \pm \dot{Q}(1 - T_0/T) \pm \dot{W} \quad (4)$$

The exergy carried by the stream can be expressed as:

$$\dot{\chi} = \dot{m}[h - h_0 - T_0(s - s_0)] \quad (5)$$

where h_0 and s_0 stand for the enthalpy and entropy at the reference temperature and pressure, respectively. $\dot{Q}$ is the heat exchanged between the component and a heat source, T is the temperature of heat source (K), and the $\dot{W}$ is the input power or output power of the system components.

The total exergy destruction can be obtained by:

$$\dot{\chi}_{\mathrm{D,total}} = \dot{\chi}_{\mathrm{D,\ com.}} + \dot{\chi}_{\mathrm{D,con.}} + \dot{\chi}_{\mathrm{D,\ CE1}} + \dot{\chi}_{\mathrm{D,\ CE2}} + \dot{\chi}_{\mathrm{D,\ EV1}} + \dot{\chi}_{\mathrm{D,\ EV2}} + \dot{\chi}_{\mathrm{D,\ EV3}} + \dot{\chi}_{\mathrm{D,\ EV4}} + \dot{\chi}_{\mathrm{D,eva.}} \quad (6)$$

The percentage of contribution of the total exergy destruction in each component:

$$\beta_{\mathrm{D},i} = \dot{\chi}_{\mathrm{D},i}/\dot{\chi}_{\mathrm{D,total}} \quad (7)$$

The exergy efficiency of the ARC is calculated as:

$$\psi = 1 - \dot{\chi}_{\mathrm{D,total}}/\dot{W}_{\mathrm{com.}} \quad (8)$$

The exergy and exergy conservation equations of the system components are shown as Table 1.

Basic conditions

Based on the above assumptions and models, the commercial software Aspen Plus 11.0 [46] is used to calculate the thermodynamic performance of the two cycles under the given operating conditions. The thermal properties of each state point in the system are calculated using the Redlich–Kwong–Aspen equation of state [47]. The environmentally benign ternary zeotropic mixture R1234yf/R170/R14 is used as the working fluid. The influence of the operating parameters on system performance will be evaluated. Table 2 lists the basic operating parameters for all the simulations below.

Simulation results and discussion

The initial composition

Usually, ternary mixtures are used in the three-stage ARC system to obtain refrigeration temperatures below − 80 °C. Calm [51] pointed out that refrigerants with low GWP value, such as R41, R170, R1132a and R1150, could be good replacements for R23 (GWP:12,000) with the standard boiling point around, ternary mixtures are used 80 °C. R1234yf is one of the most suitable replacements for R134a (GWP: 1430) [35, 36]. The standard boiling point of R14 is − 128.05 °C and can be used to obtain an evaporating temperature around − 100 °C. Thus, the ternary mixture of R1234yf/R170/R14 was chosen as the working fluid in the

Table 2 Input parameter values assumed in the simulation models

Parameter	Value
Reference temperature/T_0 (K)	298.15
Reference pressure/p_0 (kPa)	101.325
Suction pressure/p_1 (MPa)	0.2 [48]
Exhaust pressure/p_2 (kPa)	2 [48]
Mass flow rate at compressor inlet/$\dot{m}_1$ (kg/s)	1 [10]
Vapor quality at state point 8/q_8	0.5 [9]
Isentropic efficiency of compressor/$\eta_{\mathrm{com.}}$	0.8 [36, 37]

Table 1 Equations for exergy and exergy analysis [45]

Component	Energy balance	Exergy balance
com.	$\dot{W}_{\mathrm{com.}} = \dot{m}_1(h_2 - h_1) = \dot{m}_1(h_{2,\mathrm{is}} - h_1)/\eta_{\mathrm{com.}}$	$\dot{\chi}_{\mathrm{D,com.}} = \dot{m}_1 T_0(s_2 - s_1)$
con.	$\dot{Q}_{\mathrm{con.}} = \dot{m}_1(h_2 - h_3)$	$\dot{\chi}_{\mathrm{D,con.}} = \dot{m}_1 T_0(s_3 - s_2) + \dot{Q}_{\mathrm{con}}(1 - T_0/T_3)$
EV1	$h_3 = h_4$	$\dot{\chi}_{\mathrm{D},EV1} = \dot{m}_5 T_0(s_4 - s_3)$
EV2	$h_5 = h_6$	$\dot{\chi}_{\mathrm{D},EV2} = \dot{m}_5 T_0(s_6 - s_5)$
EV3	$h_9 = h_{10}$	$\dot{\chi}_{\mathrm{D},EV3} = \dot{m}_9 T_0(s_{10} - s_9)$
EV4	$h_{12} = h_{13}$	$\dot{\chi}_{\mathrm{D},EV4} = \dot{m}_{12} T_0(s_{13} - s_{12})$
CE1	$\dot{Q}_{CE1} = \dot{m}_7(h_7 - h_8) = \dot{m}_1(h_1 - h_{17})$	$\dot{\chi}_{\mathrm{D},CE1} = \dot{m}_7[(h_7 - h_8) - T_0(s_7 - s_8)] + \dot{m}_1[(h_{17} - h_1) - T_0(s_{17} - s_1)]$
CE2	$\dot{Q}_{CE2} = \dot{m}_{11}(h_{11} - h_{12}) = \dot{m}_{16}(h_{16} - h_{15})$	$\dot{\chi}_{\mathrm{D},CE2} = \dot{m}_{11}[(h_{11} - h_{12}) - T_0(s_{11} - s_{12})] + \dot{m}_{15}[(h_{15} - h_{16}) - T_0(s_{15} - s_{16})]$
eva.	$\dot{Q}_{\mathrm{eva.}} = \dot{m}_{13}(h_{14} - h_{13})$	$\dot{\chi}_{\mathrm{D,eva.}} = T_0[\dot{m}(s_{14} - s_{13}) - \frac{\dot{Q}_{\mathrm{eva.}}}{T_{\mathrm{ave}} + \Delta T}]$

where T_{ave} is the mathematic average temperature of the refrigerant at the inlet and outlet of the evaporator (K), and ΔT represents the temperature difference between the refrigerant and the cooled space, which is assumed to be 10 K

MTARC [50]. Table 3 lists the thermodynamic properties of the three pure refrigerants concerned [52].

In the operation process of the MTARC, the saturated liquid at state point 5 and state point 12 are R1234yf/R170-enriched mixture and R170/R14-enriched mixture, respectively. Thus, the initial composition of R1234yf/R170/R14 can be determined by combining the compositions of R1234yf/R170 and R170/R14. Figure 2a and b are the isobaric three-dimensional equilibrium diagram and isothermal-isobaric ternary equilibrium diagram of R1234yf/R170/R14, respectively. As shown in Fig. 2b, the bubble-surface and the dew-surface intersect with S1 at Line-1 and Line-2, respectively, since the condensation temperature is about 30 °C. Thus, the mass ratio of R1234yf/R170 can be obtained, which is about z_1 = 0.815/0.185 [18]. Similarly, the mass ratio of z_2 = 0.425/0.575 for R170/R14 can be obtained according to the intersection line between the S2 and the bubble-surface. Consequently, the initial composition of 0.65/0.15/0.20 for R1234yf/R170/R14 can be calculated.

The performance comparison under a typical operating condition

Apart from the assumptions mentioned above and the input parameters listed in Table 1, the condenser outlet quality q_3 and the intermediate pressure p_4 are set as 0.65 and 1.5 MPa, respectively. In order to better compare the refrigeration performance, the mixture at the evaporator outlet is assumed to be saturated vapor (q_{14} = 1). Under this typical operating condition, thermodynamic characteristics of the MTARC and CTARC are calculated using the ternary mixture of R1234yf/R170/R14 (0.65/0.15/0.20) and are listed in Table 4.

From Table 4, we can see that the compressor input power of the MTARC is moderately greater than that of the CTARC, while the MTARC has a much larger cooling capacity. There are two factors that affect the input power, namely the refrigerant enthalpy at the compressor inlet and the compression ratio. As shown in Table 4, the quality in the separator will increase under the effect of intermediate pressure, and then the refrigerant enthalpy at the compressor inlet and the mass flow rate in the evaporator both increase, resulting in the increase of input power and cooling capacity

Table 3 Physical properties of the alternative refrigerants

Refrigerant	Chemical name	Molecular weight/kg mol^{-1}	ODP	GWP$_{100\text{-yr}}$ (CO_2-eq)	ASHRAE safety group	NBP(°C)
R1234yf	2,3,3,3-tetrafluoropropene	114.04	0	< 1	A2L	− 29.45
R170	Ethane	30.07	0	5.5	A3	− 88.58
R14	Tetrafluoromethane	88.01	0	6630	A1	− 128.05

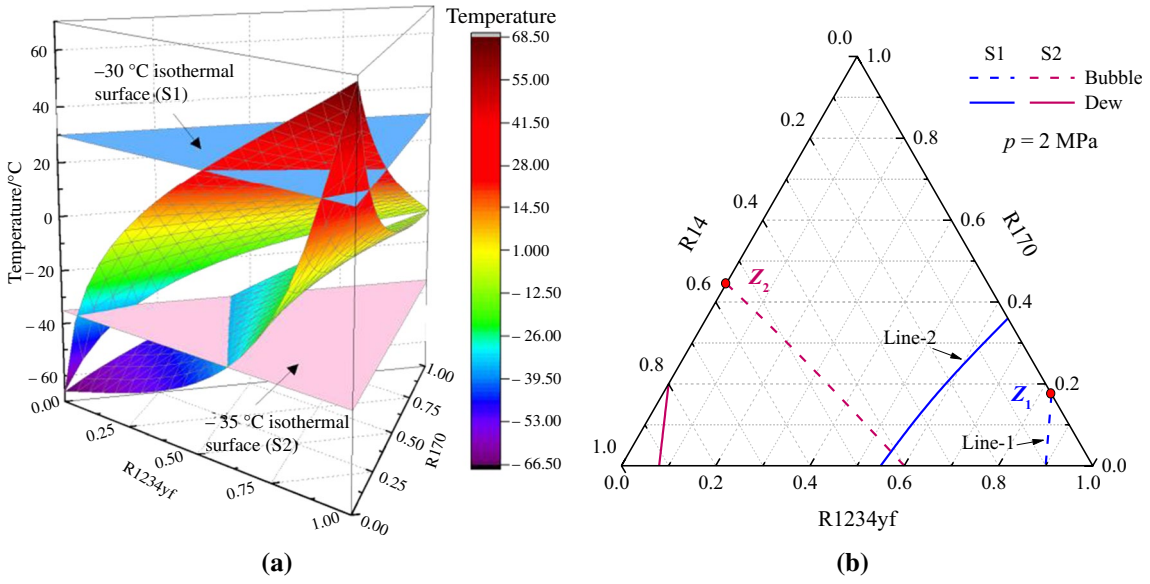

Fig. 2 **a** Isobaric three-dimensional phase equilibrium diagram at 2 MPa; **b** Isothermal-isobaric ternary phase equilibrium diagram of R1234yf/R170/R14

Table 4 The performance comparisons between two cycles under the typical operating condition

Properties	CTARC	MTARC	Improvements
Input power (kW)	108.75	112.78	–
Cooling capacity (kW)	48.57	56.27	15.85%
COP	0.4467	0.4989	11.69%
Temperature (°C)			
Evaporator inlet	−89.67	−93.32	−3.65
Evaporator outlet	−50.76	−52.43	−1.67
Compressor inlet	−11.47	−2.71	8.76
Compressor outlet	92.27	101.29	9.02
Mass flow rate (kg/s)			
$\dot{m}_7$	0.5953	0.6394	7.41%
$\dot{m}_{11}$	0.2682	0.2830	5.52%
Composition Z_{13}	0.2577/0.2288/0.5135	0.2342/0.2387/0.5271	–
Total exergy destruction (kW)	67.12	66.31	1.21%
Exergy efficiency (%)	38.28	41.20	7.65%

of the MTARC. Consequently, the COP of MTARC reaches 0.4989, which is 11.69% higher than that of the CTARC. In addition, both the evaporator inlet and outlet temperatures of the MTARC are lower than those of the CTARC. This is because the mass fraction of the volatile component R14 is increased due to the increase of quality, thus the evaporating temperatures decrease when the evaporating pressure is fixed. However, the suction and exhaust temperatures of the MTARC are about 10 °C higher than that of the CTARC. It indicates that the MTARC can effectively prevent the compressor from liquid hammering under special circumstances. Compared with the CTARC, the MTARC has a smaller total exergy destruction and a greater input power. Consequently, the exergy efficiency of the MTARC is increased by 7.65%.

According to the operation process of the MTARC, it was found that the specific enthalpies of the refrigerant at the condenser outlet and *VLS1* inlet are equal, but the temperature and pressure at the *VLS1* inlet are greatly decreased. This is due to the effect of the isenthalpic throttling process of *EV1*. Therefore, when the suction and discharge pressures are fixed, the mass flow rate of the refrigerant in the low temperature circuit is increased due to the increase of quality at the *VLS1* inlet. Besides, the mass fraction of the low boiling point component in the evaporator will not be decreased. That is, the cooling capacity and COP of the MTARC are increased without increasing the evaporating temperature. Thus, under the premise of ensuring no liquid in the compressor suction, the cycle performance can be improved when the suction and discharge pressures are fixed.

Effect of quality q_3 on the system performance

In order to acquire an appropriate mass flow of the R170/R14-enriched refrigerant, the mixture should be partially condensed in the condenser. Thus, the refrigerant quality q_3 at the condenser outlet is limited. By ensuring no liquid existence in the compressor suction and a proper exhaust temperature, the system performance was investigated under the q_3 range of 0.58–0.75, and the refrigerant at the evaporator outlet is also assumed to be saturated vapor ($q_{14}=1$). The results show that the evaporating temperatures of the MTARC are always lower than those of the CTARC within the entire q_3 range. On the other hand, the compressor outlet temperature of the MTARC is higher than that of the CTARC. This means that the refrigerant temperature at the compressor inlet also increases, which can effectively prevent liquid hammer of the compressor.

Figure 3 shows the effect of quality q_3 on the cooling capacity, COP, total exergy destruction and exergy efficiency. From Fig. 3a we can see that the cooling capacities of both the MTARC and CTARC increase with increasing q_3. This is due to the increase of the mass flow of the refrigerant mixture in the evaporator. When q_3 is 0.75, the cooling capacity and compressor input power of the MTARC are 65.51 kW and 126.87 kW, respectively, which are 31.04% and 24.67% greater than those of 49.99 kW and 101.76 kW when q_3 is 0.58, respectively. That is, the growth rate of the cooling capacity is significantly higher than that of the input power. As a result, the COP gradually increases with increasing q_3 as shown in Fig. 3a. On the other hand, the cooling capacity and COP of the MTARC are always greater than those of the CTARC within the entire q_3 range as shown in Fig. 3b. Similar to the variation trend of the cooling capacity and COP, the total exergy destruction and exergy efficiency of the two cycles monotonically increase with increasing q_3. Besides, the total exergy destruction of the MTARC is always slightly less than that of the CTARC, while the exergy efficiency of the MTARC is much higher than that of the CTARC under the same q_3. This is because the input power of the MTARC is higher than that of the CTARC, resulting in the higher exergy efficiency according to Eq. (8). When q_3 is 0.58 and 0.75, the exergy efficiency

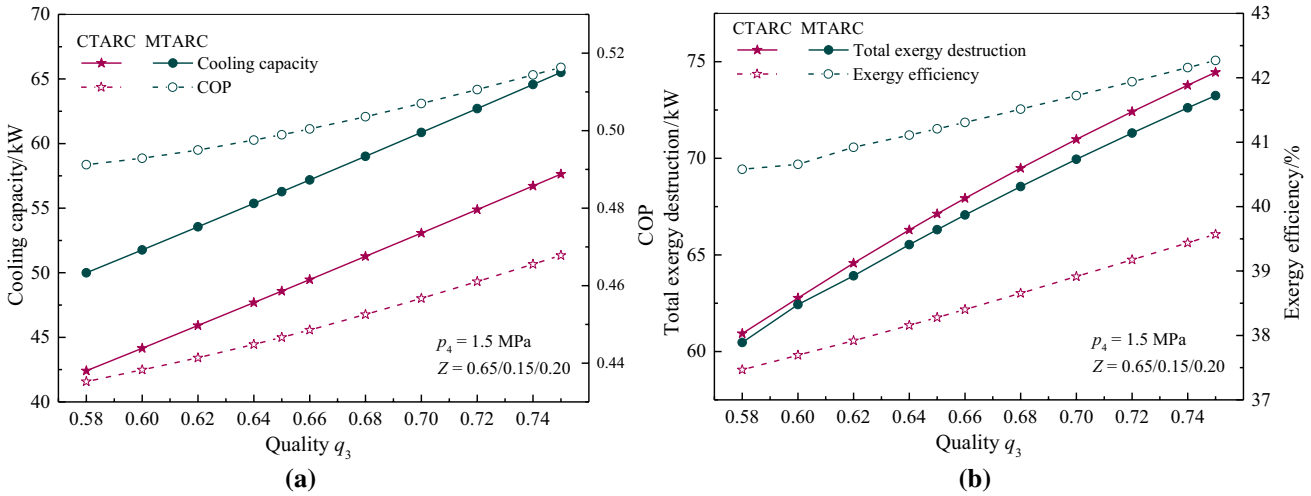

Fig. 3 **a** Effect of quality q_3 on the cooling capacity and COP; **b** Effect of quality q_3 on the total exergy destruction and exergy efficiency

of the MTARC is 40.58% and 42.27% respectively, while those of the CTARC are 37.47% and 39.57%, respectively.

Effect of initial composition on the system performance

Since the strong zeotropic mixture has a large temperature glide when evaporating at a constant pressure, it is necessary to study the system performance of the two cycles with different initial compositions. In this section, the mixture at the evaporator outlet is assumed to be saturated vapor ($q_{14}=1$). The calculated results show that the discharge temperatures of the two cycles monotonically increase with increasing initial mass fraction of R1234yf ($Z_{R1234yf}$), but decrease with increasing initial mass fraction of R14 (Z_{R14}). In addition, the compressor discharge temperature of the MTARC is higher than that of the CTARC at each initial composition. However, the evaporating temperatures of the two cycles decrease with increasing $Z_{R1234yf}$ and Z_{R14}. The reason is that the increase of $Z_{R1234yf}$ will reduce the mass fraction of R170 (Z_{R170}), which leads to the increase of the R14 mass fraction in the R170/R14-enriched mixture at state point 7. Then, the R14 mass fraction in the refrigerant mixture entering the evaporator is further increased when the quality at state point 8 (q_8) is fixed as 0.5. On the other hand, the evaporator inlet temperatures of the MTARC is about 4 °C lower than that of the CTARC at each initial composition.

Figure 4 illustrates the variations of the cooling capacity and COP of the two cycles with different initial compositions. As shown in Fig. 4a, the cooling capacities of the two

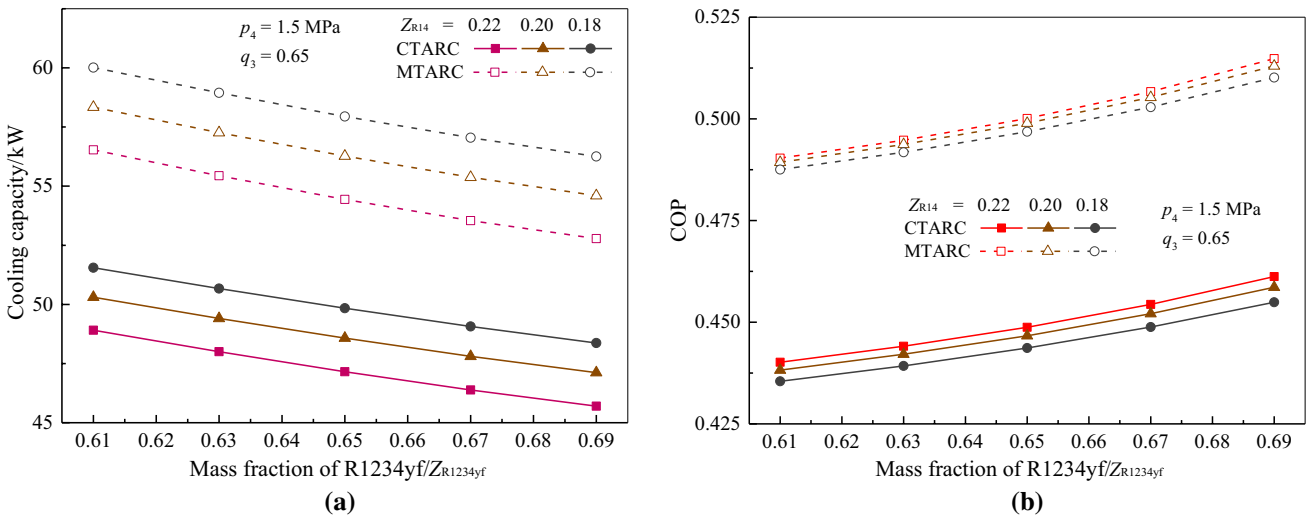

Fig. 4 **a** Effect of composition on cooling capacity; **b** Effect of composition on COP of the MTARC and CTARC

cycles decrease gradually with increasing $Z_{R1234yf}$ and Z_{R14}. In addition, the cooling capacities of the MTARC are always greater than those of the CTARC within the entire composition range. When the initial composition of R1234yf/R170/R14 is 0.61/0.21/0.18, the MTARC has a cooling capacity of 60.01 kW, which is 16.41% greater than that of 51.55 kW for the CTARC. Contrary to the variation trend of the cooling capacity, the COP of the two cycles increase with increasing $Z_{R1234yf}$ and Z_{R14}. According to Eq. (3), it indicates that the decrease rate of input power is higher than that of cooling capacity. When the initial composition of R1234yf/R170/R14 is 0.69/0.09/0.22, the MTARC has a COP of 0.5148, which is 11.62% higher than that of 0.4612 for the CTARC as shown Fig. 4b. When Z_{R14} is 0.20, the cooling capacity of the MTARC increases by 4.84% from 0.4893 to 0.5130 as $Z_{R1234yf}$ increases from 0.61 to 0.69.

Figure 5 shows the effects of initial composition on the total destruction and exergy efficiency of the two cycles. We can see from Fig. 5a that the total exergy destruction of both the MTARC and CTARC decrease gradually with increasing $Z_{R1234yf}$ and Z_{R14}. Although the input power also decreases with increasing $Z_{R1234yf}$ and Z_{R14}, the growth rate is smaller than that of the total exergy destruction. As a result, the exergy efficiency increases with increasing $Z_{R1234yf}$ and Z_{R14} as shown in Fig. 5b. Within the entire composition range, the exergy efficiencies of the MTARC are always higher than those of the CTARC, which indicates that the additional pressure regulator can significantly reduce the exergy loss of the system. When the initial composition of R1234yf/R170/R14 is 0.69/0.09/0.22, the MTARC has an exergy efficiency of 44.35%, which is 7.33% higher than that of 41.32% for the CTARC.

Effect of evaporating temperature on the system performance

The evaporating temperature is of great significance in influencing the performance of refrigeration systems. Figure 6a and b show the effects of evaporator outlet temperature T_{14} on the compressor temperature, cooling capacity, COP and exergy efficiency under the given operating conditions. As shown in Fig. 6a, all the temperatures increase gradually with increasing T_{14}, and both the compressor inlet and outlet temperatures of the MTARC are higher than those of the CTARC. It should be noted that the liquid refrigerant exists at the compressor inlet of the MTARC when T_{14} is below − 75 °C, while the compressor of the CTARC will suck liquid when T_{14} is below − 70 °C. This demonstrates that the MTARC can acquire lower evaporating temperaure without liquid hammering of the compressor. In addition, the quality q_{14} at the evaporator outlet decreases with decreasing T_{14}, which indicates that there is less liquid mixture evaporating in the evaporator. As a result, the cooling capacities of the two cycles decrease with decreasing T_{14} as shown in Fig. 6b. When T_{14} drops from − 55 to − 75 °C, the cooling capacity of the MTARC deceases by 42.66% from 52.74 kW to 30.24 kW. Meanwhile, the input power decreases by 11.20% from 110.95 to 98.52 kW. Consequently, the COP is decreased by 35.44% from 0.4754 to 0.3069. On the other hand, the performances of the MTARC are better than those of the CTARC in all given T_{14} ranges. When T_{14} is − 65 °C, the cooling capacity and COP of the MTARC are 41.41 kW and 0.3949 respectively, which show 28.20% and 17.98% improvements over the CTARC, respectively.

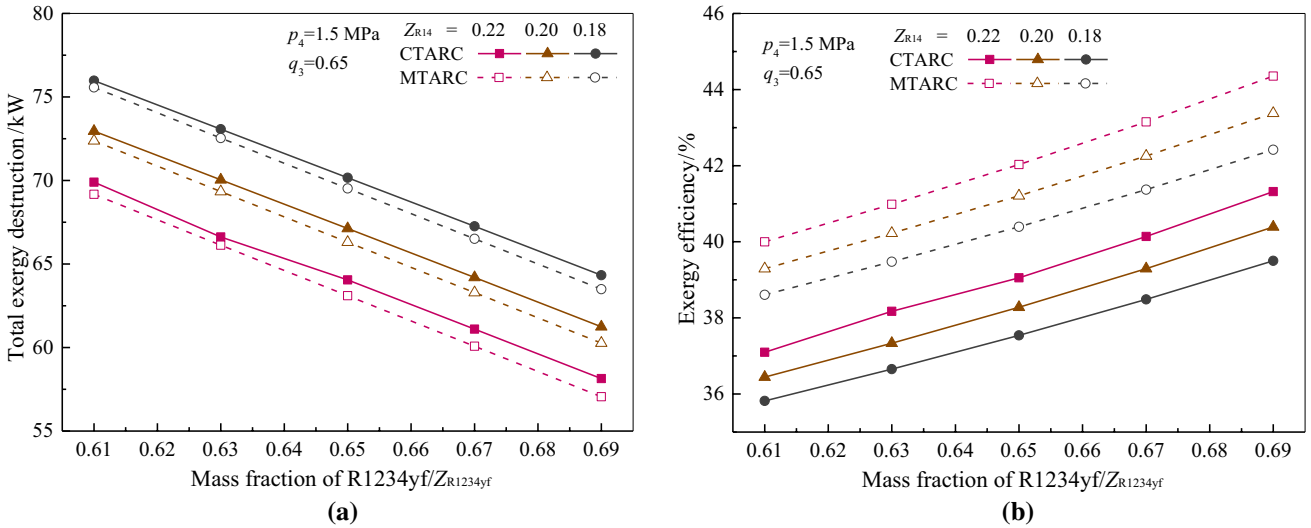

Fig. 5 **a** Effect of composition on total exergy destruction; **b** Effect of composition on exergy efficiency of the MTARC and CTARC

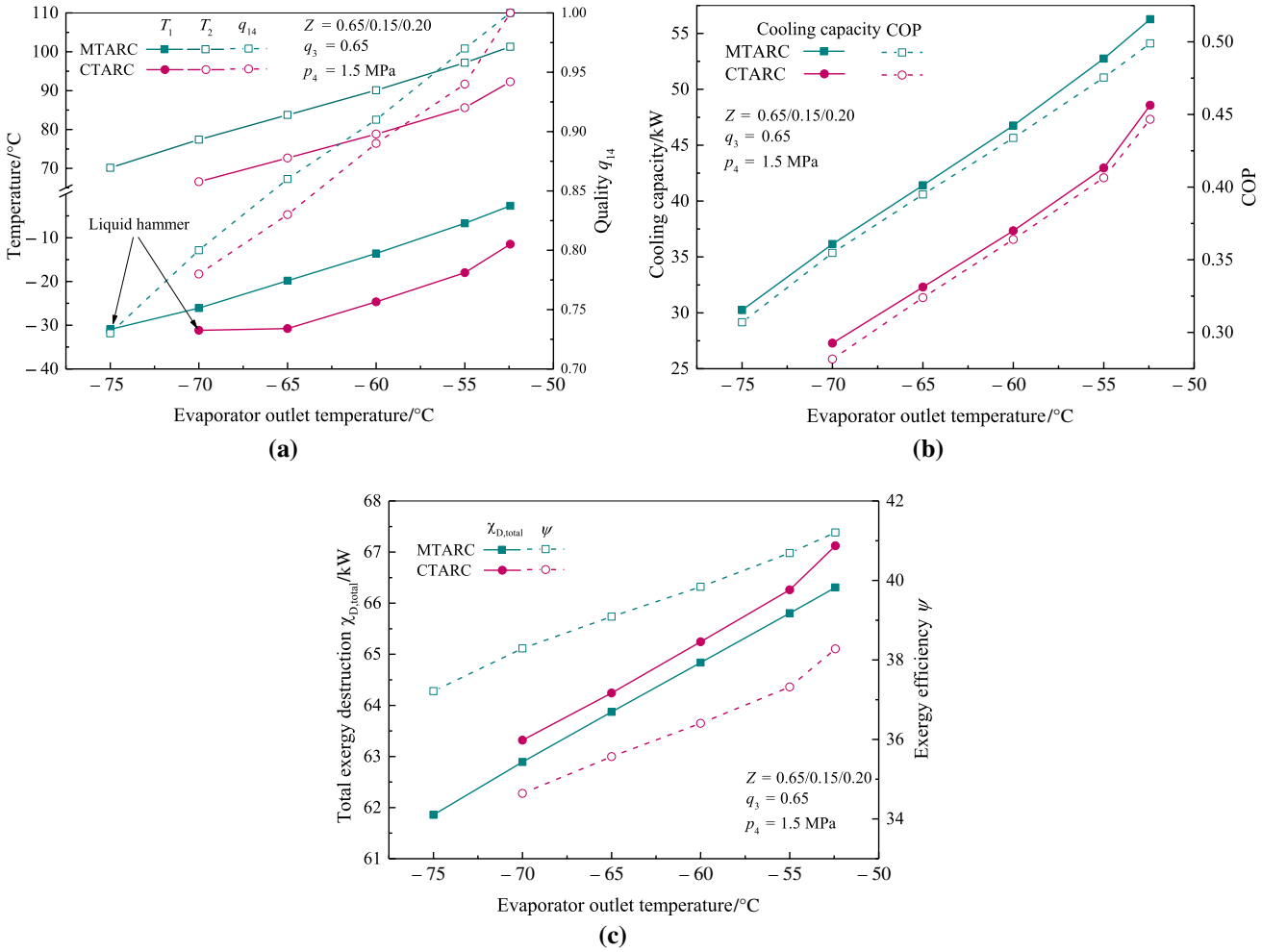

Fig. 6 **a** Effect of evaporator outlet temperature on T_1, T_2, and q_{14}; **b** Effect of evaporator outlet temperature on cooling capacity and COP; **c** Effect of evaporator outlet temperature on total exergy destruction and exergy efficiency

Figure 6c displays the variation trend of exergy performance with respect to T_{14}. Both the total exergy destruction and exergy efficiency of the two cycles gradually increase with increasing T_{14}. This indicates that the decrease rate of the total exergy destruction is greater than that of the total input power. Besides, the total exergy destructions of the MTARC are less, while the exergy efficiencies are higher than those of the CTARC within the entire T_{14} range. According to Eq. (8), the exergy efficiency is inversely proportional to the total exergy destruction, while is proportional to the input power. Therefore, it can be concluded that the MTARC can significantly reduce the input power of the compressor. This is because the pressure ratio is fixed as a constant, and the specific enthalpy difference of refrigerant at the compressor inlet and outlet of the MTARC is less than that of the CTARC. When T_{14} is − 65 °C, the exergy efficiency of the MTARC is improved by 9.89%, while that is improved by 9.03% when T_{14} is − 55 °C.

Effect of intermediate pressure on the MTARC performance

Under the action of the additional *EV1*, an intermediate pressure is obtained, and the relative independence between the refrigerant at *VLS1* inlet and the refrigerant at condenser outlet is further realized. Therefore, it is possible for the MTARC to improve the system performance. Figure 7 shows the effect of intermediate pressure p_4 on the thermodynamic performance of the MTARC under the premise of no liquid existence at the compressor inlet. In this section, the mixture at evaporator outlet is also assumed to be saturated vapor (q_{14} = 1). From Fig. 7a we can see that when p_4 drops from 2 to 1 MPa, the refrigerant temperature T_4 at *VLS1* inlet decreases by 20.38 °C, while the quality q_4 at the *VLS1* inlet increases gradually. Thus, the mass flow of the refrigerant entering the low-temperature circuit (Streams 7 and 11) is further increased as shown in Fig. 7b. As a result, the cooling capacity of the

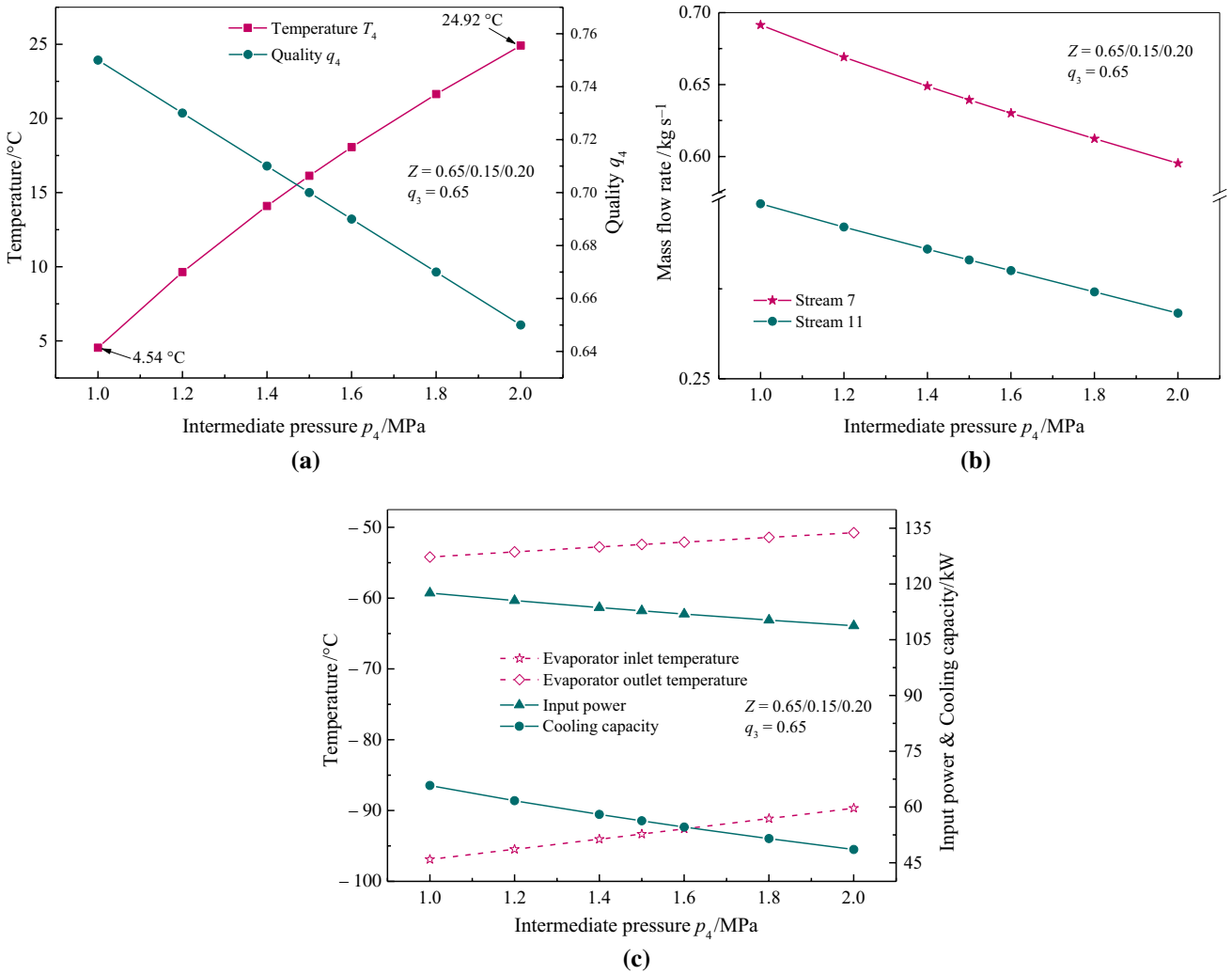

Fig. 7 **a** Effect of intermediate pressure on temperature (T_4) and quality (q_4) at *VLS1* inlet; **b** Effect of intermediate pressure on mass flow rate; **c** Effect of intermediate pressure on evaporating temperature, input power and cooling capacity

MTARC increases with decreasing p_4 as shown in Fig. 7c. As q_4 increases, the increase of the specific enthalpy of the refrigerant at compressor inlet increases, accounting for the increase of input power. Finally, the MTARC shows an improvement of 35.43% in cooling capacity when p_4 drops from 2 to 1 MPa. In addition, the evaporating temperatures also decrease with decreasing p_4. When p_4 drops from 2 to 1 MPa, the evaporator inlet temperature decreases by 7.23 °C from − 89.67 to − 96.90 °C, and the evaporator outlet temperature decreases by 3.43 °C from − 50.76 to − 54.19 °C.

Figure 8 illustrates the effect of intermediate pressure on the compressor outlet temperature, COP and exergy efficiency of the MTARC. Clearly, the decreasing p_4 results in an increase of COP and exergy efficiency. This is because the growth rate of the cooling capacity is larger than that of the input power, which leads to an increase of COP. When the pressure is 1.2 MPa, the COP reaches 0.5340, and the compressor outlet temperature is

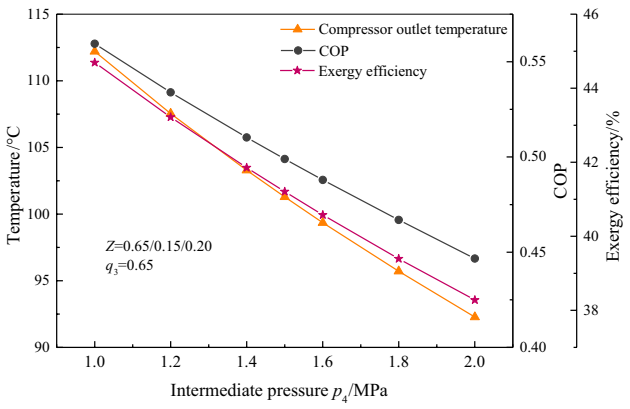

Fig. 8 Effect of intermediate pressure on compressor outlet temperature, COP and exergy efficiency of the MTARC

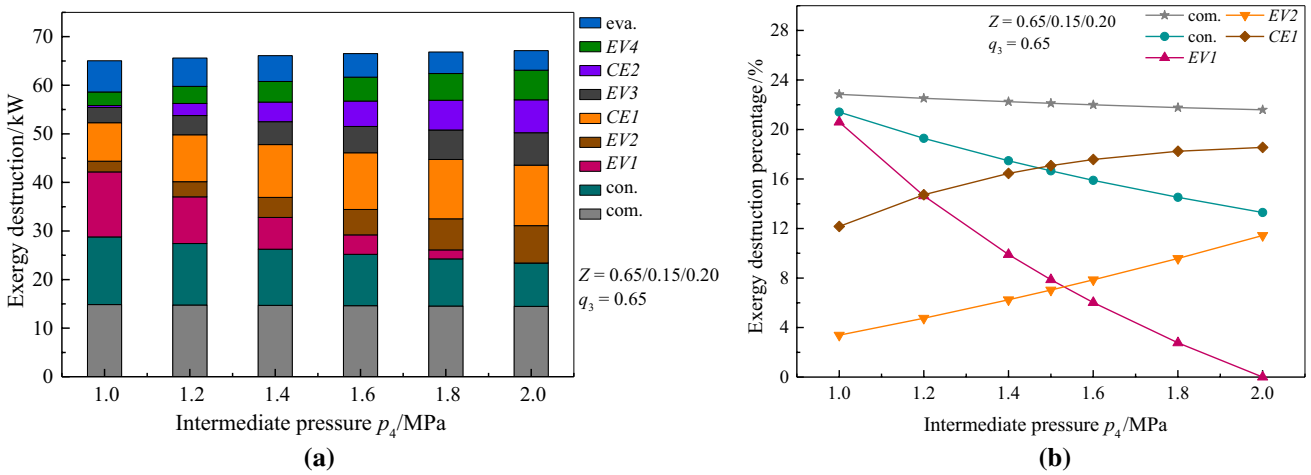

Fig. 9 **a** Effect of intermediate pressure on exergy destruction; **b** Effect of intermediate pressure on exergy destruction percentage

107.54 °C, which is an appropriate operating temperature. When p_4 drops from 2 to 1 MPa, the COP and exergy efficiency are improved by 25.25% and 16.74%, respectively. However, the compressor outlet temperature increases by 19.93 °C from 92.27 to 112.20 °C. The reason is that the quality in the separator increases as p_4 decreases, which leads to the increase of vapor refrigerant mass flowing to the low-temperature circuit (Steam 7 and 11) and the decrease of liquid refrigerant mass flow at state point 5. Because the quality at the evaporator outlet is fixed as 1, the mixed refrigerant at state points 17 and 15 cannot provide sufficient cooling capacity to condense the vapor refrigerant. As a result of the comprehensive effect, the temperature of the refrigerant at the compressor inlet increases, further increasing the discharge temperature. Therefore, the selection of the intermediate pressure should be comprehensively considered to ensure a desirable thermodynamic performance and a proper working temperature of the compressor in actual applications.

In order to determine the main locations of irreversibility in the MTARC, the effect of p_4 on the exergy destruction and exergy destruction percentage of each system component are depicted in Fig. 9. It can be seen from Fig. 9a that when p_4 drops to 1 MPa, the compressor, condenser and *EV1* contribute the most to the exergy destruction. With decreasing p_4, the exergy destruction percentages of the condenser and *EV1* increase gradually as show in Fig. 9b. This is attributed to the increase of heat transfer temperature difference in the condenser and the pressure drop in the *EV1*. On the contrary, the exergy destruction percentages of the *CE1* and *EV2* decrease with decreasing p_4, while those of the compressor remain almost constant. This indicates that the exergy efficiency of the MTARC can be further improved mainly by enhancing the heat transfer performance of condenser and the structural optimization of *EV1*.

Conclusions

At present, the studies related to the performance analysis of the ARC mainly focus on the improvement of separation efficiency, in which the decrease of the refrigerant flow to the evaporator was not considered. In order to solve this problem and propose an efficient refrigeration cycle to obtain the refrigeration temperatures around − 80 °C, this paper introduces a pressure regulator into a modified three-stage ARC, which can effectively decrease the refrigerant pressure and temperature in the separator to obtain a high separation efficiency, and can increase the vapor quality and the refrigerant flow to the evaporator. The environmentally benign ternary mixture of R1234yf/R170/R14 was used as the working fluid for sustainability concerns. Energy and exergy analyses of the CTARC and MTARC are conducted theoretically considering the key operating parameters of the composition, quality and intermediate pressure. The foregoing analysis results indicate that the MTARC is meaningful and manifest significant performance improvements. Major conclusions drawn from this research are summarized as follows:

(1) The MTARC can effectively increase the refrigerant flow rate to the evaporator, which rendering the MTARC always shows significantly better performance than the CTARC. Under a typical working condition, the cooling capacity, COP and exergy efficiency of the MTARC are improved by 15.85%, 11.69% and 7.65% comparing with those of the CTARC, respectively.

(2) As the mass fraction of the less volatile component increases, the cooling capacity of two cycles are deteriorated, while the COP and exergy efficiency are increased due to the decline of the compressor input power. When the initial composition of R1234yf/R170/R14 is 0.69/0.09/0.22, the COP and exergy efficiency of

the MTARC are 11.62% and 7.33% higher than those of the CTARC, respectively.

(3) As the quality at condenser outlet increases, the COP, cooling capacity and exergy efficiency of the two cycles are improved gradually. When the quality is 0.75, the COP and exergy efficiency of MTARC are 10.25% and 6.82% higher than those of the CTARC.

(4) The performance of the MTARC is improved with decreasing intermediate pressure. When the intermediate pressure drops from 2 to 1 MPa, the cooling capacity, COP and exergy efficiency of the MTARC are improved by 35.43%, 25.25% and 16.74%, respectively, while the compressor outlet temperature increases by 19.93 °C from 92.27 to 112.20 °C. Therefore, the selection of the intermediate pressure should be comprehensively considered to ensure a desirable thermodynamic performance and a proper working temperature for the compressor in actual applications.

In general, the MTARC can offer many advantages for its applications in low-temperature equipment down to − 80 °C, such as freezers, cryopreservation chamber, and the pre-cooling system for cryoablation devices. Because many assumptions were adopted in the modeling process, the analytical results still show some deviation from the actual operating conditions and the MTARC only verifies its improvements in theory. Thus, further experimental work will be necessary in the next step before practical application. Besides, the exergy analysis suggests that the heat transfer enhancement of the air-cooled condenser and the structure optimization of the throttle valves are the key improvements of the ARC systems.

Acknowledgements This work was financially supported by the National Natural Science Foundation of China (Grant No. 51906151), and the China Postdoctoral Science Foundation (Grant No. 2019M661572).

Author contributions The specific contributions to this work of each author are listed as follows, which has been agreed by all authors. YQ contributed to software, investigation, writing—original draft, writing—review & editing, and funding acquisition. NL contributed to validation, investigation, and writing—review & editing. HZ contributed to methodology and supervision. BL contributed to conceptualization and resources.

Declarations

Conflict of interest The authors declare that there is no financial and personal relationships with other people or organizations that can inappropriately influence our work, there is no professional or other personal interest of any nature or kind in any product, service and/or company that could be construed as influencing the position presented in, or the review of, the manuscript entitled "Energy and exergy evaluation of a modified three-stage auto-cascade refrigeration system using low-GWP refrigerants for sustainable development".

References

1. Mota-Babiloni A, Mastani Joybari M, Navarro-Esbrí J, Mateu-Royo C, Barragán-Cervera Á, Amat-Albuixech M, et al. Ultralow-temperature refrigeration systems: configurations and refrigerants to reduce the environmental impact. Int J Refrig. 2020;111:147–58.
2. Rodríguez-Jara EÁ, Sánchez-de-la-Flor FJ, Expósito-Carrillo JA, Salmerón-Lissén JM. Thermodynamic analysis of auto-cascade refrigeration cycles, with and without ejector, for ultra low temperature freezing using a mixture of refrigerants R600a and R1150. Appl Therm Eng. 2022;200:117598.
3. Johnson N, Baltrusaitis J, Luyben WL. Design and control of a cryogenic multi-stage compression refrigeration process. Chem Eng Res Des. 2017;121:360–7.
4. Wang Q, Li DH, Wang JP, Sun TF, Han XH, Chen GM. Numerical investigations on the performance of a single-stage auto-cascade refrigerator operating with two vapor–liquid separators and environmentally benign binary refrigerants. Appl Energy. 2013;112:949–55.
5. Harby K. Hydrocarbons and their mixtures as alternatives to environmental unfriendly halogenated refrigerants: an updated overview. Renew Sustain Energy Rev. 2017;73:1247–64.
6. Qin Y, Li N, Zhang H, Liu B. Thermodynamic performance of a modified −150 °C refrigeration system coupled with Linde-Hampson and three-stage auto-cascade using low-GWP refrigerants. Energy Convers Manag. 2021;236:114093.
7. Sarkar J. Ejector enhanced vapor compression refrigeration and heat pump systems—a review. Renew Sustain Energy Rev. 2012;16:6647–59.
8. Lawrence N, Elbel S. Theoretical and practical comparison of two-phase ejector refrigeration cycles including First and Second Law analysis. Int J Refrig. 2013;36:1220–32.
9. Yan G, Chen J, Yu J. Energy and exergy analysis of a new ejector enhanced auto-cascade refrigeration cycle. Energy Convers Manag. 2015;105:509–17.
10. Tan Y, Wang L, Liang K. Thermodynamic performance of an auto-cascade ejector refrigeration cycle with mixed refrigerant R32 + R236fa. Appl Therm Eng. 2015;84:268–75.
11. Boyaghchi FA, Asgari S. A comparative study on exergetic, exergoeconomic and exergoenvironmental assessments of two internal auto-cascade refrigeration cycles. Appl Therm Eng. 2017;122:723–37.
12. Hao X, Wang L, Wang Z, Tan Y, Yan X. Hybrid auto-cascade refrigeration system coupled with a heat-driven ejector cooling cycle. Energy. 2018;161:988–98.
13. Yu J, Zhao H, Li Y. Application of an ejector in autocascade refrigeration cycle for the performance improvement. Int J Refrig. 2008;31:279–86.
14. Bai T, Yan G, Yu J. Experimental investigation of an ejector-enhanced auto-cascade refrigeration system. Appl Therm Eng. 2018;129:792–801.
15. Bai T, Yan G, Yu J. Experimental investigation on the dynamic malfunction behavior of the two-phase ejector in a modified auto-cascade freezer refrigeration system. Energy Convers Manag. 2019;183:382–90.
16. Cheng Z, Wang B, Shi W, Li X. Performance evaluation of novel double internal auto-cascade two-stage compression system using refrigerant mixtures. Appl Therm Eng. 2020;168:114898.
17. Chen Q, Zhou L, Yan G, Yu J. Theoretical investigation on the performance of a modified refrigeration cycle with R170/R290 for freezers application. Int J Refrig. 2019;104:282–90.
18. Sobieraj M, Rosiński M. High phase-separation efficiency auto-cascade system working with a blend of carbon dioxide

for low-temperature isothermal refrigeration. Appl Therm Eng. 2019;161:114149.
19. Yu M, Yu J. Thermodynamic analyses of a flash separation ejector refrigeration cycle with zeotropic mixture for cooling applications. Energy Convers Manag. 2021;229:113755.
20. Zhang L, Xu S, Du P, Liu H. Experimental and theoretical investigation on the performance of CO2/propane auto-cascade refrigerator with a fractionation heat exchanger. Appl Therm Eng. 2015;87:669–77.
21. Chen J, Yu J, Yan G. Performance analysis of a modified autocascade refrigeration cycle with an additional evaporating subcooler. Appl Therm Eng. 2016;103:1205–12.
22. Liu J, Liu Y, Yan G, Yu J. Theoretical study on a modified single-stage autocascade refrigeration cycle with auxiliary phase separator. Int J Refrig. 2021;122:181–91.
23. Mei B, Barnoon P, Toghraie D, Su C-H, Nguyen HC, Khan A. Energy, exergy, environmental and economic analyzes (4E) and multi-objective optimization of a PEM fuel cell equipped with coolant channels. Renew Sustain Energy Rev. 2022;157:112021.
24. Ahmadi G, Toghraie D, Akbari OA. Efficiency improvement of a steam power plant through solar repowering. Int J Exergy. 2017;22:1.
25. Ahmadi GR, Toghraie D. Energy and exergy analysis of Montazeri steam power plant in Iran. Renew Sustain Energy Rev. 2016;56:454–63.
26. Ma Y, Fazilati MA, Sedaghat A, Toghraie D, Talebizadehsardari P. Natural convection energy recovery loop analysis, part I: energy and exergy studies by varying inlet air flow rate. Heat Mass Transf. 2020;56:1685–95.
27. Heydari O, Miansari M, Arasteh H, Toghraie D. Optimizing the hydrothermal performance of helically corrugated coiled tube heat exchangers using Taguchi's empirical method: energy and exergy analysis. J Therm Anal Calorim. 2021;145:2741–52.
28. Adeli J, Niknejadi M, Toghraie D. Full repowering of an existing fossil fuel steam power plant in terms of energy, exergy, and environment for efficiency improvement and sustainable development. Environ Dev Sustain. 2020;22:5965–99.
29. Miansari M, Valipour MA, Arasteh H, Toghraie D. Energy and exergy analysis and optimization of helically grooved shell and tube heat exchangers by using Taguchi experimental design. J Therm Anal Calorim. 2020;139:3151–64.
30. Asgari S, Noorpoor AR, Boyaghchi FA. Parametric assessment and multi-objective optimization of an internal auto-cascade refrigeration cycle based on advanced exergy and exergoeconomic concepts. Energy. 2017;125:576–90.
31. Yan G, Hu H, Yu J. Performance evaluation on an internal auto-cascade refrigeration cycle with mixture refrigerant R290/R600a. Appl Therm Eng. 2015;75:994–1000.
32. Rezayan O, Behbahaninia A. Thermoeconomic optimization and exergy analysis of CO2/NH3 cascade refrigeration systems. Energy. 2011;36:888–95.
33. Aprea C, Maiorino A. Autocascade refrigeration system: experimental results in achieving ultra low temperature. Int J Energy Res. 2009;33:565–75.
34. Sivakumar M, Somasundaram P. Exergy and energy analysis of three stage auto refrigerating cascade system using Zeotropic mixture for sustainable development. Energy Convers Manag. 2014;84:589–96.
35. Sivakumar M, Somasudaram P. Thermodynamic investigations of Zeotropic mixture of R290, R23 and R14 on three-stage auto refrigerating cascade system. Therm Sci. 2016;20:2073–86.
36. Qin Y, Li N, Zhang H, Liu B. Energy and exergy performance evaluation of a three-stage auto-cascade refrigeration system using low-GWP alternative refrigerants. Int J Refrig. 2021;126:66–75.
37. Kilicarslan A, Hosoz M. Energy and irreversibility analysis of a cascade refrigeration system for various refrigerant couples. Energy Convers Manag. 2010;51:2947–54.
38. Lizarte R, Palacios-Lorenzo ME, Marcos JD. Parametric study of a novel organic Rankine cycle combined with a cascade refrigeration cycle (ORC-CRS) using natural refrigerants. Appl Therm Eng. 2017;127:378–89.
39. Liu J, Liu Y, Yan G, Yu J. Thermodynamic analysis on a modified auto-cascade refrigeration cycle with a self-recuperator. Int J Refrig. 2022;137:117–28.
40. Sobieraj M. Experimental investigation of the effect of a recuperative Heat exchanger and throttles opening on a CO2/isobutane autocascade refrigeration system. Energies. 2020;13:5285.
41. Rui S, Zhang H, Zhang B, Wen D. Experimental investigation of the performance of a single-stage auto-cascade refrigerator. Heat Mass Transf. 2016;52:11–20.
42. He Y, Wu H, Liu Y, Wang T, Wu X, Cheng C, et al. Theoretical performance comparison for two-stage auto-cascade refrigeration system using hydrocarbon refrigerants. Int J Refrig. 2022;142:27–36.
43. Hamad AJ, Hussien FM, Yousif SS. Comparative study of auto cascade refrigeration system performance using alternative mixed refrigerants. Int J Eng Res Ind Appl. 2015;8:111–26.
44. Chen J, Zhu K, Huang Y, Chen Y, Luo X. Evaluation of the ejector refrigeration system with environmentally friendly working fluids from energy, conventional exergy and advanced exergy perspectives. Energy Convers Manag. 2017;148:1208–24.
45. Mousavi SA, Mehrpooya M. A comprehensive exergy-based evaluation on cascade absorption-compression refrigeration system for low temperature applications-exergy, exergoeconomic, and exergoenvironmental assessments. J Clean Prod. 2020;246:119005.
46. ASPEN Plus. Aspen Technology Inc., 200 Wheeler Road Burlington, MA, USA 2020.
47. Mathias P. A versatile phase equilibrium equation of state. Ind Eng Chem Process Des Dev. 1983;22(3):385–91. https://doi.org/10.1021/i200022a008.
48. Navarro-Esbrí J, Mendoza-Miranda JM, Mota-Babiloni A, Barragán-Cervera A, Belman-Flores JM. Experimental analysis of R1234yf as a drop-in replacement for R134a in a vapor compression system. Int J Refrig. 2013;36:870–80.
49. Mendoza-Miranda JM, Mota-Babiloni A, Ramírez-Minguela JJ, Muñoz-Carpio VD, Carrera-Rodríguez M, Navarro-Esbrí J, et al. Comparative evaluation of R1234yf, R1234ze(E) and R450A as alternatives to R134a in a variable speed reciprocating compressor. Energy. 2016;114:753–66.
50. Sun Z, Wang Q, Xie Z, Liu S, Su D, Cui Q. Energy and exergy analysis of low GWP refrigerants in cascade refrigeration system. Energy. 2019;170:1170–80.
51. Calm JM. The next generation of refrigerants—historical review, considerations, and outlook. Int J Refrig. 2008;31:1123–33.
52. Lemmon EW, Huber ML, Mclinden MO. NIST Standard Reference Database 23: reference fluid thermodynamic and transport properties—REFPROP, version 9.1, Standard Reference Data Program, National Institute of Standards and Technology 2010.